

Article

A Fractional-Order Improved Quantum Logistic Map: Chaos, 0-1 Testing, Complexity, and Control

Birong Xu ^{1,*}, Ximei Ye ¹, Guangyi Wang ² , Zhongxian Huang ³ and Changwu Zhang ¹¹ College of Mechanic and Electronic Engineering, Wuyi University, Wuyishan 354300, China² Institute of Modern Circuits and Intelligent Information, Hangzhou Dianzi University, Hangzhou 310018, China³ College of Mathematics and Computer Science, Wuyi University, Wuyishan 354300, China

* Correspondence: xubirong@wuyiu.edu.cn

Abstract: Based on a quantum logistic map and a Caputo-like delta difference operator, a fractional-order improved quantum logistic map, which has hidden attractors, was constructed. Its dynamical behaviors are investigated by employing phase portraits, bifurcation diagrams, Lyapunov spectra, dynamical mapping, and 0-1 testing. It is shown that the proposed fractional-order map is influenced by both the parameters and the fractional order. Then, the complexity of the map is explored through spectral entropy and approximate entropy. The results show that the fractional-order improved quantum logistic map has stronger robustness within chaos and higher complexity, so it is more suitable for engineering applications. In addition, the fractional-order chaotic map can be controlled for different periodic orbits by the improved nonlinear mapping on the wavelet function.

Keywords: improved quantum logistic map; discrete fractional calculus; hidden attractor; chaos control

MSC: 26A33; 34H10; 39A33



Citation: Xu, B.; Ye, X.; Wang, G.; Huang, Z.; Zhang, C. A Fractional-Order Improved Quantum Logistic Map: Chaos, 0-1 Testing, Complexity, and Control. *Axioms* **2023**, *12*, 94. <https://doi.org/10.3390/axioms12010094>

Academic Editors: António Lopes, Alireza Alfi, Liping Chen and Sergio Adriani David

Received: 4 December 2022

Revised: 7 January 2023

Accepted: 10 January 2023

Published: 16 January 2023



Copyright: © 2023 by the authors. Licensee MDPI, Basel, Switzerland. This article is an open access article distributed under the terms and conditions of the Creative Commons Attribution (CC BY) license (<https://creativecommons.org/licenses/by/4.0/>).

1. Introduction

Since May presented the logistic map in 1976, and as a well-known chaotic map, the logistic map and its generalizations have gained more and more attention in academic circles, especially regarding chaos and fractals [1–3]. A quantum logistic map that is associated with the logistic map is proposed in [4]. As a three-dimensional map, it was found that the quantum logistic map owns richer dynamical behaviors, and thus it has greater potential application in the field of information security. However, when compared to the logistic map, there has been relatively less research into quantum logistic maps. The generalization of quantum logistic maps has never been analyzed, so we have investigated it.

In recent years, the theory of the fractional differential equation has become a new research focus. The author of [5] introduced fractional LTI systems, and [6] investigated the existence of a mild-solution Hilfer fractional-neutral-integro-differential inclusion with almost sectorial operators. The authors of [7] studied the existence, uniqueness, Hyer-Ulam stability, and controllability of a fractional dynamic system using time scales, and [8] analyzed the existence, uniqueness, and stability of a nonlinear fractional differential equation with impulsive conditions on time scales. The dynamics of a fractional-order model with different strains of COVID-19 were explored in [9]. The new field of fractional differential equations emerged via the discretized definitions of continuous fractional derivatives and integrals [10–13]. With the rapid development of the fractional difference equations theory, the definition of fractional-order difference was introduced into discrete chaotic maps based on the Caputo operator, and the fractional standard map and the fractional logistic map were proposed [14,15]. Since then, researchers have diverted their interest to fractional-order chaotic maps. The authors of [16–18] presented fractional-order logistic maps and fractional-order delayed logistic maps and analyzed their nonlinear

behaviors by using phase portraits, bifurcation diagrams, and Lyapunov exponents. The authors of [19] designed an efficient image encryption scheme based on the fractional-order logistic map, while those of [20] put forward a fractional-order Hénon-Lozi map and then studied its dynamical properties. A two-dimensional fractional-order map was designed and applied to image encryption [21]. A fractional-order higher-dimensional multicavity chaotic map was studied in [22]. Fractional-order chaotic maps are sensitive to their fractional order apart from their initial values and parameters, thereby having richer nonlinear behaviors than the integer-order versions. Hence, a generalized quantum logistic map with fractional order is presented in the paper.

On the other hand, the chaotic system with hidden attractors is a new research hotspot. Some chaotic systems with hidden attractors were presented in the literature [23–25]. If a chaotic system possesses no equilibrium or stable equilibrium, i.e., its attraction basin does not connect with the neighborhood of the equilibrium, the chaotic system is regarded as a chaotic system with hidden attractors [26,27]. The hidden attractor is considerably important in science and engineering due to the occurrence of unexpected behaviors. The term “hidden attractors” originates from the research of continuous chaotic systems [28,29]. When compared with continuous chaotic systems, the investigation of chaotic maps with hidden attractors has seen a lack of investigation, especially for fractional-order maps with hidden attractors; they are rarely introduced in the literature. However, the fractional-order map owns more complex dynamical behaviors than the integer counterpart. In order to enrich the theory of hidden attractors, we propose a fractional-order improved quantum logistic map without equilibrium, i.e., a fractional-order map with hidden attractors. For future applications, its behaviors are explored by nonlinear tools, such as bifurcation diagrams and Lyapunov exponents. Moreover, the chaos control of this fractional-order map is also studied.

The remainder of this paper is outlined as follows. Section 2 gives a fractional-order improved quantum logistic map. Section 3 shows the dynamical analysis of the fractional-order map by exploiting bifurcation analysis, Lyapunov exponent spectrums, dynamical maps, and 0-1 tests. Section 4 focuses on the complexity of this map. Section 5 investigates the chaos control of the system. We draw conclusions in Section 6.

2. A Fractional-Order Improved Quantum Logistic Map

A quantum logistic map is a logistic map with quantum corrections [4]. In order to investigate the effects of these quantum corrections, researchers set $\hat{a} = \langle \hat{a} \rangle + \delta \hat{a}$, where $\delta \hat{a}$ is a quantum fluctuation about $\langle \hat{a} \rangle$, and $\langle \hat{a} \rangle$ is the mean value of \hat{a} . The quantum logistic map is described as

$$\begin{cases} x_n = r(x_{n-1} - |x_{n-1}|^2) - ry_{n-1}, \\ y_n = -y_{n-1}e^{-2\beta} + e^{-\beta}r[(2 - x_{n-1} - x_{n-1}^*)y_{n-1} - x_{n-1}z_{n-1}^* - x_{n-1}^*z_{n-1}], \\ z_n = -z_{n-1}e^{-2\beta} + e^{-\beta}r[2(1 - x_{n-1}^*)z_{n-1} - 2x_{n-1}y_{n-1} - x_{n-1}], \end{cases} \quad (1)$$

where $x = \langle \hat{a} \rangle$, $y = \langle \delta \hat{a}^+ \delta \hat{a} \rangle$, $z = \langle \delta \hat{a} \delta \hat{a} \rangle$, and x^* , z^* are the complex conjugate of x , z , respectively. Besides, β and r denote the dissipation and control parameters, respectively. However, if we let the initial values x_0 , y_0 , and z_0 be real numbers, the successive values x_n , y_n , and z_n remain real. Therefore, Equation (1) is expressed as

$$\begin{cases} x_n = r(x_{n-1} - |x_{n-1}|^2) - ry_{n-1}, \\ y_n = -y_{n-1}e^{-2\beta} + e^{-\beta}r[(2 - 2x_{n-1})y_{n-1} - 2x_{n-1}z_{n-1}], \\ z_n = -z_{n-1}e^{-2\beta} + e^{-\beta}r[2(1 - x_{n-1})z_{n-1} - 2x_{n-1}y_{n-1} - x_{n-1}], \end{cases} \quad (2)$$

For the quantum logistic map, the map has one fixed-point: (0, 0, 0). In order to design a chaotic system with hidden attractors, Equation (2) is rewritten as

$$\begin{cases} x_n = f(x_{n-1}) - r_1 y_{n-1}, \\ y_n = -y_{n-1}e^{-2\beta} + e^{-\beta}r[(2 - 2x_{n-1})y_{n-1} - 2x_{n-1}z_{n-1}], \\ z_n = -z_{n-1}e^{-2\beta} + e^{-\beta}r[2(1 - x_{n-1})z_{n-1} - 2x_{n-1}y_{n-1} - x_{n-1}], \end{cases} \tag{3}$$

where r_1 is a parameter, and the function $f(x_{n-1})$ is defined as

$$f(x_{n-1}) = \begin{cases} 0.8 + rx_{n-1}(0.2 - x_{n-1}) \\ \text{if } 0 < x_{n-1} < 0.2, \\ r(x_{n-1} - 0.8)(1 - x_{n-1}) \\ \text{if } 0.8 < x_{n-1} < 1. \end{cases} \tag{4}$$

For solving the fixed-point of system (3), we have $x_n = x_{n-1}$, $y_n = y_{n-1}$, and $z_n = z_{n-1}$, that is

$$\begin{cases} x_n = f(x_n) - r_1 y_n, \\ y_n = -y_n e^{-2\beta} + e^{-\beta}r[(2 - 2x_n)y_n - 2x_n z_n], \\ z_n = -z_n e^{-2\beta} + e^{-\beta}r[2(1 - x_n)z_n - 2x_n y_n - x_n], \end{cases} \tag{5}$$

where the function $f(x)$ is described as

$$f(x_n) = \begin{cases} 0.8 + rx_n(0.2 - x_n) \text{ if } 0 < x_n < 0.2, \\ r(x_n - 0.8)(1 - x_n) \text{ if } 0.8 < x_n < 1. \end{cases} \tag{6}$$

The solution of Equation (5) has two cases. When $0 < 0.8 + rx_n(0.2 - x_n) - r_1 y_n < 0.2$ or $0.8 < r(x_n - 0.8)(1 - x_n) - r_1 y_n < 1$, the first equation can be solved, i.e., the fractional-order map has a fixed-point. If not, there is no solution to the first equation. In other words, the improved map is a system without equilibrium. The second case will be considered below.

Regarding the second and third equations as fractional order, we can obtain

$$\begin{cases} x_n = f(x_{n-1}) - r_1 y_{n-1}, \\ {}^C\Delta_a^\nu y(t) = -y(t + \nu - 1)e^{-2\beta} + e^{-\beta}r[(2 - 2x(t + \nu - 1))y(t + \nu - 1) \\ - 2x(t + \nu - 1)z(t + \nu - 1)] - y(t + \nu - 1), \\ {}^C\Delta_a^\nu z(t) = -z(t + \nu - 1)e^{-2\beta} + e^{-\beta}r[2(1 - x(t + \nu - 1))z(t + \nu - 1) \\ - 2x(t + \nu - 1)y(t + \nu - 1) - x(t + \nu - 1)] - z(t + \nu - 1), \end{cases} \tag{7}$$

where ${}^C\Delta_a^\nu$ is the ν -th Caputo-like delta difference operator, ν is the fractional order, and a is the starting point. Set N_a is the isolated time scale, $N_a = \{a, a + 1, a + 2, \dots\}$ ($a \in \mathbb{R}$ fixed). For $\nu > 0$, $\nu \notin \mathbb{N}$, and $u(t)$ define on N_a , the Caputo-like delta difference [30] is defined by

$${}^C\Delta_a^{-\nu} u(t) = \Delta_a^{-(m-\nu)} \Delta^m u(t), t \in N_{a+m-\nu}, m = [\nu] + 1, \tag{8}$$

where ν is the difference order and $\Delta_a^{-(m-\nu)}$ is the fractional sum of $m-\nu$ order. Let $u: N_a \rightarrow \mathbb{R}$ and $\nu > 0$, the fractional sum of ν order [10] is defined by

$$\Delta_a^{-\nu} u(t) = \frac{1}{\Gamma(\nu)} \sum_{s=a}^{t-\nu} (t - \sigma(s))^{(\nu-1)} u(s), t \in N_{a+\nu}, \tag{9}$$

where $\sigma(s) = s + 1$, $\Gamma(\nu)$ is the Gamma function, and $t(\nu)$ is the falling function defined by the Gamma function as

$$t^{(\nu)} = \frac{\Gamma(t + 1)}{\Gamma(t + 1 - \nu)}. \tag{10}$$

Therefore, the Caputo-like delta difference can be expressed as

$${}^C\Delta_a^{-\nu}u(t) = \frac{1}{\Gamma(m-\nu)} \sum_{s=a}^{t-(m-\nu)} (t-\sigma(s))^{(m-\nu-1)} \Delta^m u(s), t \in \mathbb{N}_{a+m-\nu}, = [\nu] + 1. \tag{11}$$

According to the theorem in [31], for the difference equation:

$$C\Delta_a^\nu u(t) = f(t + \nu - 1, u(t + \nu - 1)), \Delta^k u(a) = u_k, m = [\nu] + 1, k = 0, \dots, m - 1. \tag{12}$$

The equivalent discrete integral equation is described as

$$u(n) = u_0(t) + \frac{1}{\Gamma(\nu)} \sum_{s=a+m-\nu}^{t-\nu} (t-\sigma(s))^{(\nu-1)} \times f(s + \nu - 1, u(s + \nu - 1)), t \in \mathbb{N}_{a+m}, \tag{13}$$

where the initial iteration is

$$u_0(t) = \sum_{k=0}^{m-1} \frac{(t-a)^{(k)}}{k!} \Delta^k u(a). \tag{14}$$

By setting $m = 1, a = 0$, and substituting $\sigma(s) = s + 1$ into Equation (13), the following can be obtained as

$$u(n) = u_0(t) + \frac{1}{\Gamma(\nu)} \sum_{s=1-\nu}^{t-\nu} (t-s-1)^{(\nu-1)} \times f(s + \nu - 1, u(s + \nu - 1)) \tag{15}$$

By using Equation (10), and setting $j = s + \nu$, Equation (15) is rewritten as

$$u(n) = u_0(t) + \frac{1}{\Gamma(\nu)} \sum_{j=1}^n \frac{\Gamma(n-j+\nu)}{\Gamma(n-j+1)} \times f(j-1, u(j-1)) \tag{16}$$

According to Equation (16), the explicit numerical formula of Equation (7) is expressed as

$$\begin{cases} x_n = f(x_{n-1}) - r_1 y_{n-1}, \\ y_n = y_0 + \frac{1}{\Gamma(\nu)} \sum_{j=1}^n \frac{\Gamma(n-j-\nu)}{\Gamma(n-j-1)} \{-y_{j-1} e^{-2\beta} + e^{-\beta} r [(2 - 2x_{j-1})y_{j-1} - 2x_{j-1}z_{j-1}] - y_{j-1}\}, \\ z_n = z_0 + \frac{1}{\Gamma(\nu)} \sum_{j=1}^n \frac{\Gamma(n-j-\nu)}{\Gamma(n-j-1)} \{-z_{j-1} e^{-2\beta} + e^{-\beta} r [2(1 - x_{j-1})z_{j-1} - 2x_{j-1}y_{j-1} - x_{j-1}] - z_{j-1}\}, \end{cases} \tag{17}$$

where the function $f(x_{n-1})$ is the same as Equation (4).

For System (17), set the parameters as $r = 19.8, r_1 = 0.05, \beta = 4.5$, and $\nu = 0.90$, and the initial conditions as (0.05, 0.02, and 0.05); the chaotic attractors are depicted in Figure 1, which are hidden attractors (see Appendix A for the code of the simulation). In this case, we obtain the largest Lyapunov exponent $LLE = 0.5426$ via the wolf algorithm.

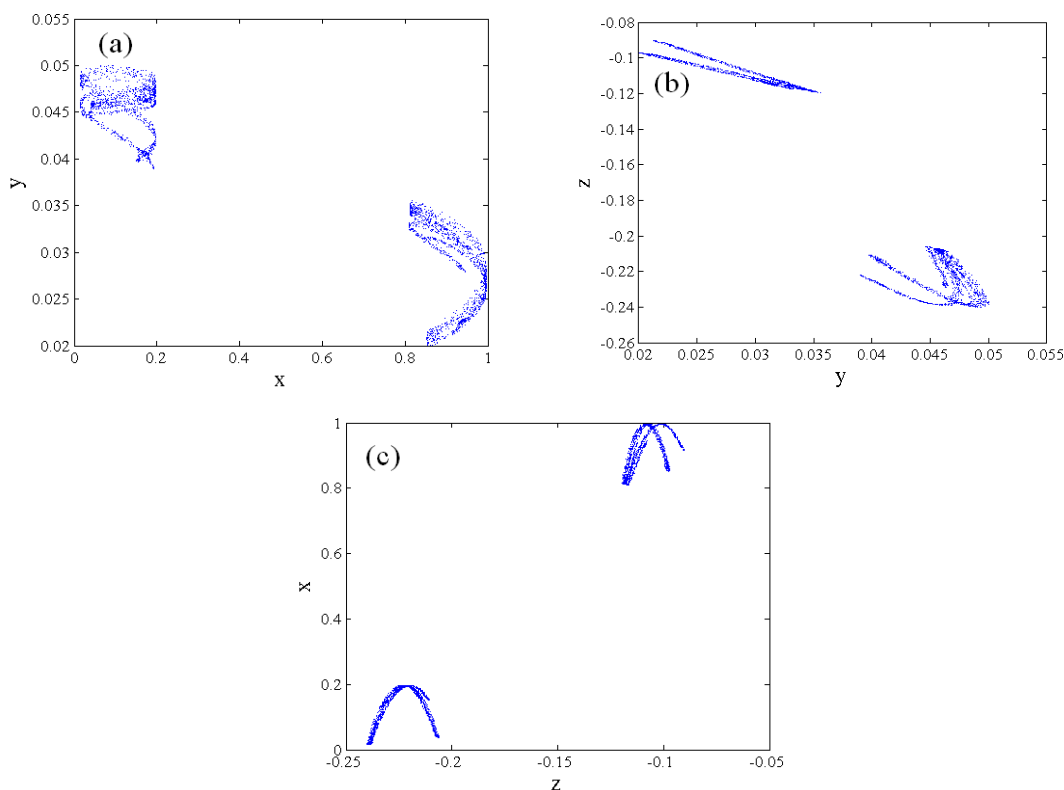


Figure 1. Chaotic attractors of the fractional-order improved quantum logistic map. (a) x - y phase portrait; (b) y - z phase portrait; (c) z - x phase portrait.

3. Dynamical Analysis

3.1. Bifurcation Analysis, Lyapunov Exponent Spectrum, and Dynamical Map

Chaotic maps have sensitivity to the parameters. In order to investigate the sensitivity of the parameters, we fixed the initial conditions as (0.05, 0.02, and 0.05). The bifurcation portrait with respect to the control parameter r and the corresponding largest Lyapunov spectrum is depicted in Figure 2, where the parameter r is in the interval [16,21], and the others are $r_1 = 0.05$, $\beta = 4.5$, and $\nu = 0.9$. It is clear to see that the bifurcation portrait is divided into two parts. With an increase in the parameter r , the system goes through period-2, period-4, a quasi-periodic, and a chaotic state. The system generates periodic windows of different sizes after the system appears in a chaotic state. In the region of $19.2 \leq r \leq 20$, the system keeps a chaotic state.

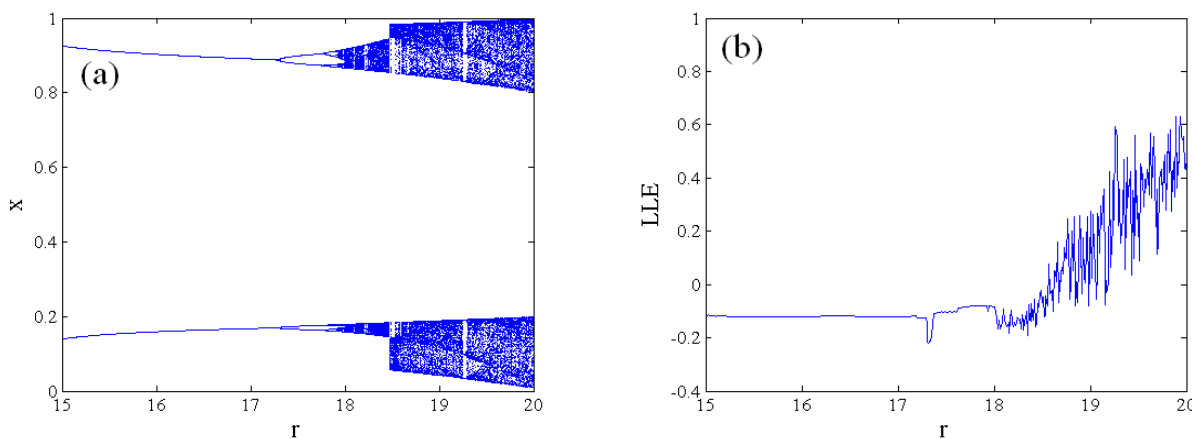


Figure 2. Bifurcation portrait and Lyapunov exponent spectrum with regard to r ; (a) bifurcation portrait with regard to r ; (b) Lyapunov exponent spectrum with regard to r .

For the dissipation parameter β , the bifurcation portrait and largest Lyapunov spectrum are plotted in Figure 3 with $r = 19.8$, $r_1 = 0.05$, and $\nu = 0.9$. Although the bifurcation portrait shows the phenomenon of bifurcation, the map is mainly in chaotic oscillation. Its chaotic regions are wider than those of the quantum logistic map. When the parameter β is greater than 3.75, the largest Lyapunov exponent is positive, which illustrates that the fractional-order map goes into chaos. When $\beta \in (3.75, 8.35]$, the largest Lyapunov roughly increases with the increasing parameter β . In the range of 8.35 to 15, the largest Lyapunov varies around 5.5. Some of the largest Lyapunov exponents exceed 6, indicating that the map has good nonlinearity and is suitable for information encryption.

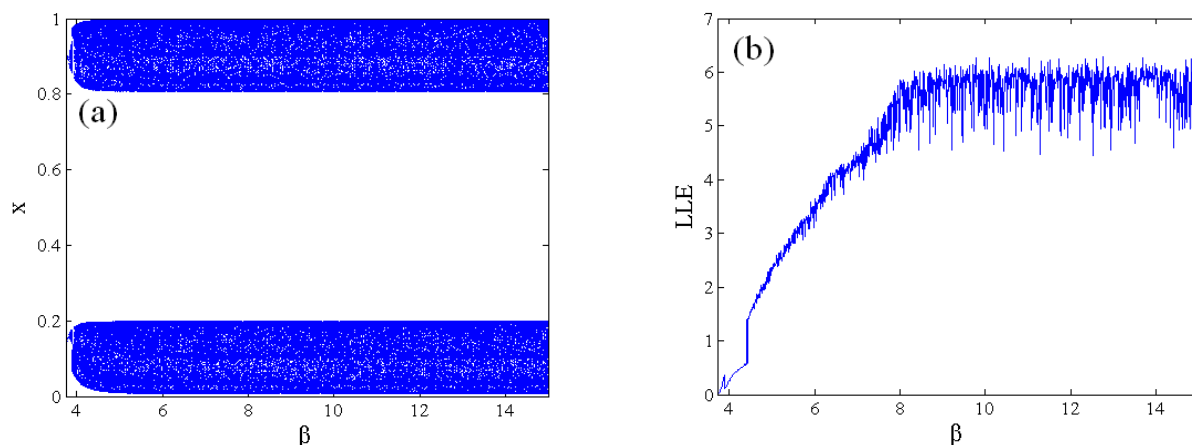


Figure 3. Bifurcation portrait and Lyapunov exponent spectrum with regard to β . (a) Bifurcation portrait with regard to β ; (b) Lyapunov exponent spectrum with regard to β .

Next, we analyze how the fractional order ν influences the map. Figure 4 presents the bifurcation portrait and Lyapunov spectrum versus ν , where the parameters are set as $r_1 = 0.05$, $\beta = 4.5$, $r = 1.98$, and $0.326 \leq \nu \leq 1$. As can be seen from Figure 4, the largest Lyapunov exponent is always greater than zero, which means that the map remains chaotic. Unlike some other fractional-order chaotic maps [32,33], there are no periodic windows in the chaotic region. Further, the magnitude of the variable $x(n)$ hardly changes with the varying of the fractional order ν . This map demonstrates stronger robustness during chaos than the fractional-order logistic map, the fractional-order Hénon map, and the other fractional-order chaotic maps in [32,33]. When the fractional order is $\nu < 0.326$, the iteration value may not be in the domain of definition. If the iterative value is not in the domain of definition, the iteration will stop. In particular, the phase portrait shows finite points under the condition of $\nu = 0.2$, as shown in Figure 5a, which implies that the iteration stops. On the contrary, Figure 5b exhibits the chaotic attractors with $\nu = 0.5$. However, these chaotic attractors are different from the chaotic attractors shown in Figure 1. The analysis illustrates that the fractional-order map owns richer dynamical behaviors than the integer counterpart.

In order to investigate the influence of the parameters and fractional order on the fractional-order map simultaneously, the dynamical maps are depicted in Figure 6, where the color represents the value of the largest Lyapunov exponent. Figure 6a illustrates the impacts of the control parameters and fractional orders when $r_1 = 0.05$, $\beta = 10$, and $(x_0, y_0, z_0) = (0.05, 0.02, 0.05)$. It is clear to see that the fractional-order map undergoes a change from periodic oscillation to chaos with increasing fractional order. Figure 6b visualizes the influences of the dissipation parameters and fractional orders, where the parameters are set as $r = 5$ and $r_1 = 0.05$, and the initial condition is chosen as $(x_0, y_0, z_0) = (0.05, 0.02, 0.05)$. The effects of the dissipation parameters and fractional orders are different from those of the control parameters and fractional orders. The largest Lyapunov exponent in most of the areas is greater than zero, i.e., the system is mainly in a chaotic state.

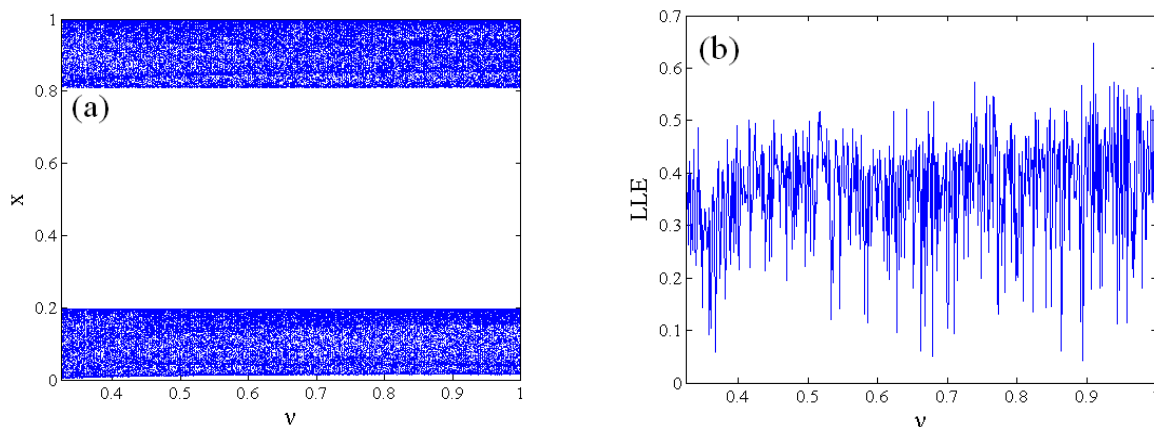


Figure 4. Bifurcation portrait and Lyapunov exponent spectrum with regard to ν . (a) Bifurcation portrait with regard to ν ; (b) Lyapunov exponent spectrum with regard to ν .

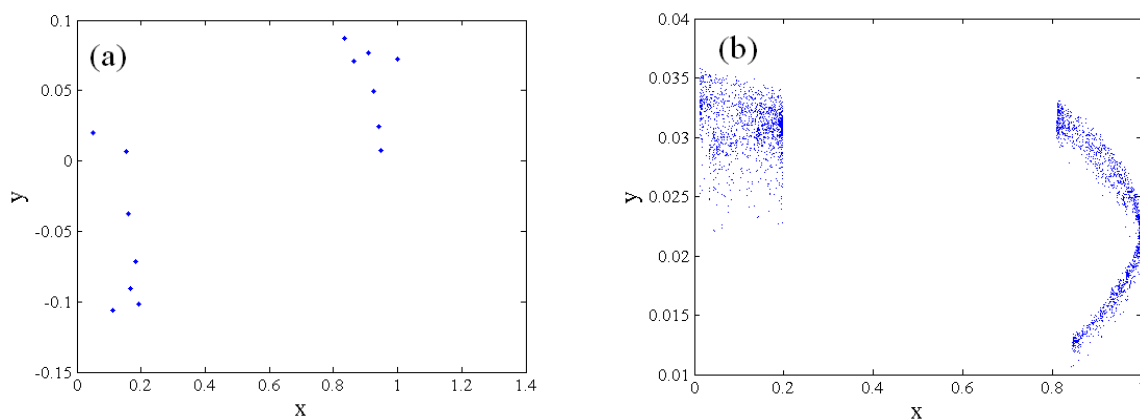


Figure 5. Phase portrait. (a) Phase portrait with $\nu = 0.2$; (b) phase portrait with $\nu = 0.5$.

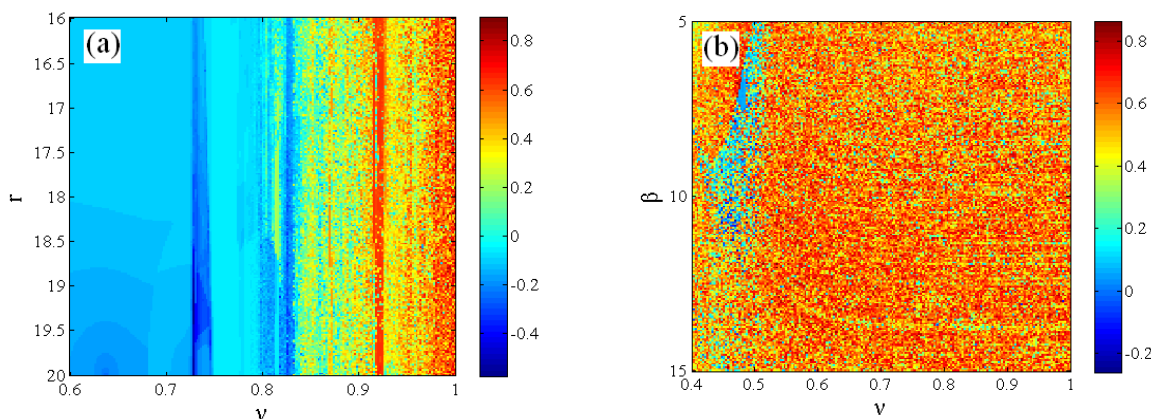


Figure 6. Dynamical maps. (a) Dynamical map with regard to ν and r ; (b) dynamical map with regard to ν and β .

3.2. 0-1 Test

The 0-1 test is another approach to verify the existence of chaos, which can be utilized directly to a series of data without any phase space reconstruction [34]. Based on the state $\{x(j)\}$ of System (17), the translation components $p_c(n)$ and $q_c(n)$ are defined as

$$p_c(n) = \sum_{j=1}^n x(j) \cos(jc), \quad q_c(n) = \sum_{j=1}^n x(j) \sin(jc) \tag{18}$$

where c is an arbitrary constant in the interval $(0, \pi)$. By plotting the dynamics of the translation components $p_c - q_c$, it is easy to determine the state of the system. If $p - q$ trajectories are Brownian-like, the state of the system is chaotic, whereas if the trajectories are bounded, the state is periodic.

Next, the mean square displacement M_c on $p_c(n)$ and $q_c(n)$ is defined as

$$M_c = \lim_{N \rightarrow \infty} \frac{1}{N} \sum_{j=1}^N \{ [p_c(j+n) - p_c(j)]^2 + [q_c(j+n) - q_c(j)]^2 \}, \quad n \ll N, \quad (19)$$

where N is the length of time sequences. In practice, n is chosen as $N/10$, and the superscript of \sum is $N - n$.

Finally, the asymptotic growth rate K_c is calculated by

$$K_c = \lim_{n \rightarrow +\infty} \frac{\log M_c}{\log n}. \quad (20)$$

We get 100 values for K_c and then let $K = \text{median}(K_c)$. When the value of K approaches 0, the system is in a periodic state, and when this value approaches 1, the system is chaotic.

The 0-1 test is performed, and the asymptotic growth rate, K , against r is depicted in Figure 7 under the conditions of $r_1 = 0.05$, $\beta = 4.5$, $\nu = 0.9$, and $(x_0, y_0, z_0) = (0.05, 0.02, 0.05)$. The asymptotic growth rate K is consistent with the bifurcation portrait and the largest Lyapunov spectrum shown in Figure 2. In order to further illustrate the nonlinear behaviors, the $p - q$ trajectories are demonstrated in Figure 8. When $r = 17$, the bounded trajectory of the $p - q$ plane is shown in Figure 8a, and the asymptotic growth rate is $K = 0.0001$, implying that the system state is periodic. On the contrary, as $r = 19.8$, the Brownian-like trajectory is presented in Figure 8b, and the asymptotic growth rate is obtained as $K = 0.9958$, illustrating that the state is chaotic. Furthermore, the chaotic sequences of $r = 19.8$ are divided into two sequences according to the value of x_n . The trajectories of $0 < x_n < 0.2$ and $0.8 < x_n < 1$ are plotted in Figure 8c,d, respectively. The trajectories demonstrate that two sequences keep a chaotic state, so the map can produce multiple chaotic sequences.

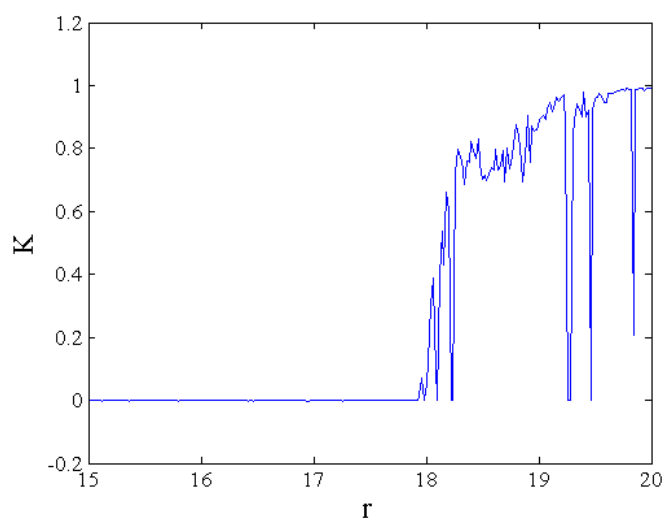


Figure 7. Asymptotic growth rate K of the fractional-order map with regard to r .

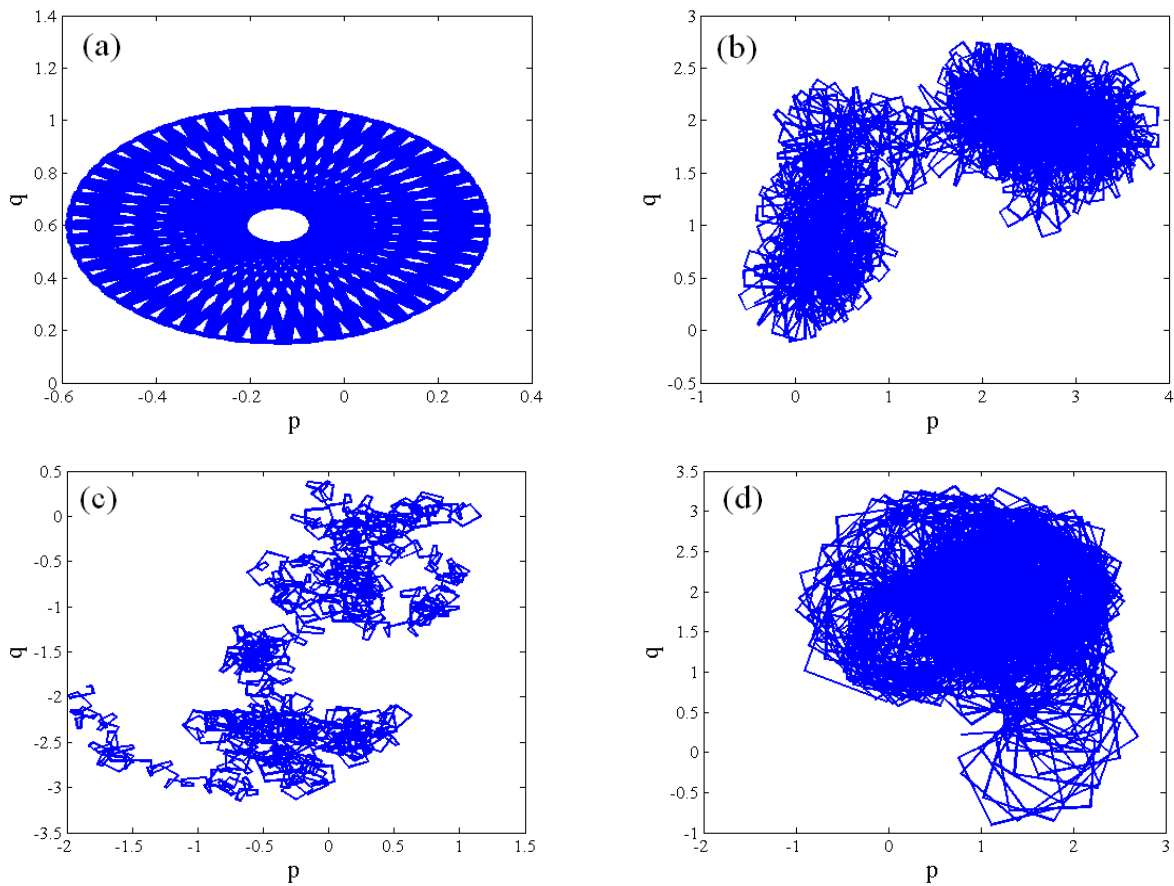


Figure 8. The p - q trajectories of the fractional-order map. (a) p - q trajectories of $r = 17$; (b) the p - q trajectories of $r = 19.8$; (c) p - q trajectories of $0 < x_n < 0.2$; (d) p - q trajectories of $0.8 < x_n < 1$.

4. Complexity and Entropy

4.1. Spectral Entropy

Complexity is an index that is used to measure how well a chaotic system generates random sequences, and larger complexity implies more randomness for the generated sequences. The complexity of the fractional-order map is evaluated by means of spectral entropy (SE). The spectral entropy algorithm [35] is defined as follows; consider a set of time sequences $\{x_n, n = 0, 1, 2, \dots, N - 1\}$ with a length of N , and obtain a new discrete number of length N by subtracting the mean of this dataset, which is expressed as

$$x_n = x_n - \frac{\sum_{n=0}^{N-1} x_n}{N}, \tag{21}$$

The Fourier transformation is calculated by

$$X_k = \sum_{n=0}^{N-1} x_n e^{-j2n\pi k/N}, \tag{22}$$

where $k = 0, 1, 2, \dots, N - 1$ and j is the unit imaginary. The probability of the power spectrum is given as

$$P_k = \frac{|X_k|^2}{\sum_{k=0}^{N/2-1} |X_k|^2}, \tag{23}$$

Then, the normalization spectral entropy is defined as

$$SE = \frac{\sum_{k=0}^{N/2-1} |P_k \ln(P_k)|}{\ln(N/2)} \tag{24}$$

We utilize spectral entropy to measure the complexity of the fractional-order map, and the result of SE complexity is presented in Figure 9. The SE complexity surpasses 0.85 in the highest range, so this fractional-order map can generate better random sequences.

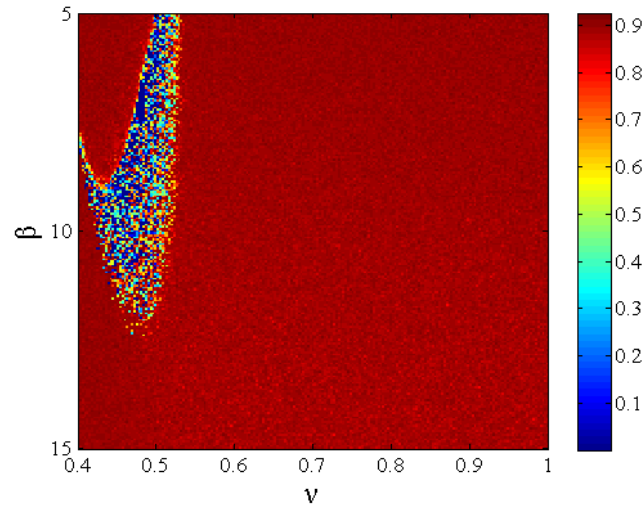


Figure 9. SE of the fractional-order map with regard to ν and β .

4.2. Approximate Entropy

The approximate entropy (ApEn) [36] is the other means to measure the complexity of the fractional-order map, which is described as follows. Consider a set of time sequences x_1, x_2, \dots, x_n obtained from System (17) and determine $n - m + 1$ vectors as follows:

$$X_i = [x_i, x_{i+1} \cdots x_{i+m-1}]. \tag{25}$$

These vectors denote m consecutive x values, which start from the i th data. Giving tolerance, r , and for each $i \in [1, n - m + 1]$, we define the following equation:

$$C_i^m(r) = \frac{K}{n - m + 1}, \tag{26}$$

in which K is the number of X_i with $d(X_i, X_j) \leq r$. In this case, $d(X_i, X_j)$ represents the largest absolute difference between X_i , and X_j . We calculate the approximate entropy by

$$APEn = \phi^m(r) - \phi^{m+1}(r), \tag{27}$$

where $\phi^m(r)$ is described as

$$\phi^m(r) = \frac{1}{n - m - 1} \sum_{i=1}^{n-m+1} \log C_i^m(r), \tag{28}$$

The result of ApEn complexity is shown in Figure 10, which agrees well with SE complexity. Therefore, this fractional-order map has a more complex structure. It has higher complexity than the fractional-order logistic map and the fractional-order Hénon map.

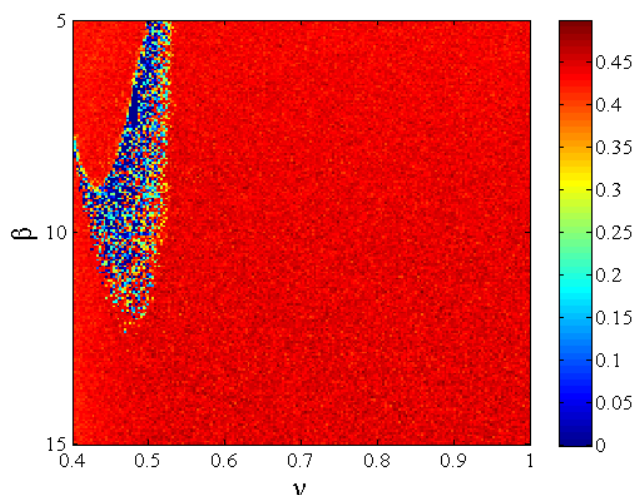


Figure 10. ApEn of the fractional-order map with regard to ν and β .

5. Chaos Control

As the fractional-order chaotic map is raised, the chaos control for the fractional-order map becomes a new topic. The occurrence of chaotic behaviors may cause instability in engineering applications, so chaos control has been widely studied. However, researchers have paid little attention to the topic of controlling fractional-order chaotic maps. In the section, the scheme of chaos control is proposed, which is based on improved nonlinear mapping on wavelet functions [37]. System (17) is controlled by it. This control method of fractional-order systems is of importance not only for control theory, but also for the application of fractional-order chaotic maps. A Marr wavelet function is employed to construct the improved nonlinear mapping. This chaos control algorithm is described as

$$\begin{cases} x_n = ke^{-\frac{x_n^2}{2}}(1 - x_{n-1}^2)[f(x_{n-1}) - r_1y_{n-1}], \\ {}^C\Delta_a^\nu y(t) = -y(t + \nu - 1)e^{-2\beta} + e^{-\beta}r[(2 - 2x(t + \nu - 1))y(t + \nu - 1) \\ \quad - 2x(t + \nu - 1)z(t + \nu - 1)] - y(t + \nu - 1), \\ {}^C\Delta_a^\nu z(t) = -z(t + \nu - 1)e^{-2\beta} + e^{-\beta}r[2(1 - x(t + \nu - 1))z(t + \nu - 1) \\ \quad - 2x(t + \nu - 1)y(t + \nu - 1) - x(t + \nu - 1)] - z(t + \nu - 1), \end{cases} \tag{29}$$

where k is a control parameter.

If System (17) is controlled when $n = 1000$, then the control results are presented in Figure 11. The fractional-order chaotic map is controlled to a period-1 orbit with $k = 0.2$; it is controlled to a period-2 orbit with $k = 0.5$, and it is controlled to period-4 orbit with $k = 0.65$, while it is controlled to quasiperiodic orbit with $k = 0.7$. As can be seen, the fractional-order chaotic map endures period-1, period-2, period-4, and quasiperiodic states with an increase in the control parameter k .

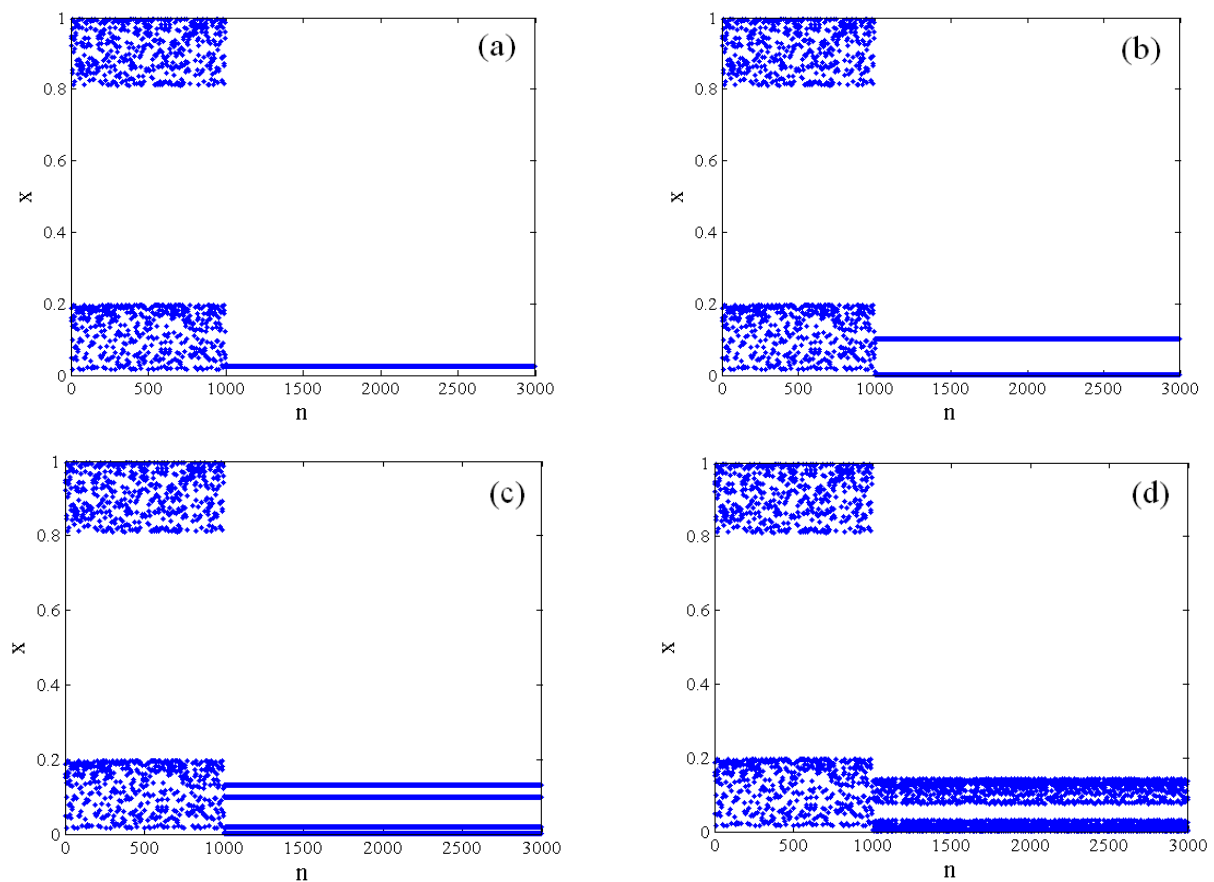


Figure 11. Chaotic controls. (a) Chaotic control with $k = 0.2$; (b) chaotic control with $k = 0.5$; (c) chaotic control with $k = 0.65$; (d) chaotic control with $k = 0.70$.

6. Conclusions

We build an improved quantum logistic map without equilibrium by reforming the classic quantum logistic map. The improved quantum logistic map with hidden attractors is generalized to the fractional case by introducing the Caputo-like delta difference operator. Through a phase portrait, the largest Lyapunov exponent, dynamical mapping, and 0-1 testing, the dynamical characteristics were studied. Both the parameters and fractional orders impact the system. With varying control parameters, the system shows periodic windows. However, for the dissipation parameter and the fractional order, there are no periodic windows in the chaotic region. This means that this chaotic map possesses stronger robustness in chaos, so the system could be applied to generate stable chaotic sequences for secure communication. The 0-1 test shows that this fractional-order map can generate several chaotic sequences. Then, the complexity of the fractional-order map was described by spectral entropy and approximate entropy, which shows that this fractional-order map can generate better random sequences. In addition, improved nonlinear mapping on a wavelet function for the fractional-order map was proposed. This map is controlled to different periodic orbits under different control parameters. The fractional-order map gains more degrees of freedom compared to the integer counterpart, so the fractional-order map has greater potential applications in the engineering field. Due to its higher complexity and stronger robustness in chaos, this fractional-order chaotic map can be employed in information encryptions, such as secret communications and image encryptions. In order to apply the fractional-order improved quantum logistic map, we will focus on designing the image encryption scheme based on this map in the future.

Author Contributions: Conceptualization, B.X. and G.W.; methodology, B.X. and G.W.; software, B.X., X.Y. and C.Z.; validation, B.X.; formal analysis, Z.H.; writing—original draft preparation, B.X. and C.Z.; writing—review and editing, X.Y., Z.H. and G.W.; supervision, G.W.; project administration, B.X.; funding acquisition, B.X., Z.H. and G.W. All authors have read and agreed to the published version of the manuscript.

Funding: This work is supported in part by the National Natural Science Foundation of China (Grant No. 61771176), the Natural Science Foundations of Fujian Province (Grant No. 2020J01395 and 2022J011203), and the innovation team of Wuyi University (Grant No. 2020-SSTD-005).

Data Availability Statement: Not applicable.

Conflicts of Interest: The authors declare that there is no conflict of interest.

Appendix A

The code generating chaotic attractors in MATLAB:

```
v=0.9;β=4.5;r=19.8;r1=0.05;
x(1)=0.05;y(1)=0.02;z(1)=0.05;
for i=2:1:3000
temp4=0;temp7=0;
for j=2:1:i temp5=temp4+exp(gammain(i-j+ν)-gammain(i-j+1))*((-y(j-1)*exp(-2*β))+
exp(-β)*r*((2-2*x(j-1))*y(j-1)-2*x(j-1)*z(j-1))-y(j-1)); temp8=temp7+exp(gammain
(i-j+ν)-gammain(i-j+1))*((-z(j-1)*exp(-2*β))+exp(-β)*r*(2*(1-x(j-1))*z(j-1)-
(2*x(j-1)*y(j-1))-x(j-1))-z(j-1));
temp4=temp5;temp7=temp8;
temp6=(1/gamma(ν))*temp5; temp9=(1/gamma(ν))*temp8;
end
if (0<x(i-1))&&(x(i-1)<0.2)
x(i)=0.8+r*(x(i-1)-0)*(0.2-x(i-1))-r1*y(i-1);
elseif (0.8<x(i-1))&&(x(i-1)<1)
x(i)=0+r*(x(i-1)-0.8)*(1-x(i-1))-r1*y(i-1);
end
y(i)=y(1)+temp6; z(i)=z(1)+temp9;
end
figure;
plot(x(100:3000),y(100:3000),'b.','markersize',2);
xlabel('x');ylabel('y');
set(gca,'fontsize',12,'FontName','Times new Roman');
set(get(gca,'XLabel'),'FontName','Times new Roman','FontSize',16);
set(get(gca,'YLabel'),'FontName','Times new Roman','FontSize',16);
figure;
plot(y(100:3000),z(100:3000),'b.','markersize',2);
xlabel('y');ylabel('z');
set(gca,'fontsize',12,'FontName','Times new Roman');
set(get(gca,'XLabel'),'FontName','Times new Roman','FontSize',16);
set(get(gca,'YLabel'),'FontName','Times new Roman','FontSize',16);
figure;
plot(z(100:3000),x(100:3000),'b.','markersize',2);
xlabel('z');ylabel('x');
set(gca,'fontsize',12,'FontName','Times new Roman');
set(get(gca,'XLabel'),'FontName','Times new Roman','FontSize',16);
set(get(gca,'YLabel'),'FontName','Times new Roman','FontSize',16);
```

References

1. May, R.M. Simple mathematical models with very complicated dynamics. *Nature* **1976**, *261*, 459–467. [[CrossRef](#)] [[PubMed](#)]
2. Munir, F.A.; Zia, M.; Mahmood, H. Designing multi-dimensional logistic map with fixed-point finite precision. *Nonlinear Dyn.* **2019**, *97*, 2147–2158. [[CrossRef](#)]
3. Cánovas, J.; Muñoz-Guillermo, M. On the dynamics of the q-deformed logistic map. *Phys. Lett. A* **2019**, *383*, 1742–1754. [[CrossRef](#)]
4. Goggin, M.; Sundaram, B.; Milonni, P. Quantum logistic map. *Phys. Rev. A* **1990**, *41*, 5705. [[CrossRef](#)]
5. Petráš, I. Fractional-order systems. In *Fractional-Order Nonlinear Systems: Modeling, Analysis and Simulation*, 1st ed.; Springer: Berlin/Heidelberg, Germany, 2011; pp. 43–54.
6. Varun Bose, C.B.S.; Udhayakumar, R. Existence of mild solutions for hilfer fractional neutral integro-differential inclusions via almost sectorial operators. *Fractal Fract.* **2022**, *6*, 532. [[CrossRef](#)]
7. Kumar, V.; Malik, M. Existence, stability and controllability results of fractional dynamic system on time scales with application to population dynamics. *Int. J. Nonlin. Sci. Num.* **2021**, *22*, 741–766. [[CrossRef](#)]
8. Kumar, V.; Malik, M. Existence, uniqueness and stability of nonlinear implicit fractional dynamical equation with impulsive condition on time scales. *Nonauton. Dyn. Syst.* **2019**, *6*, 65–80. [[CrossRef](#)]
9. Baba, I.A.; Rihan, F.A. A fractional-order model with different strains of COVID-19. *Phys. A* **2022**, *603*, 127813. [[CrossRef](#)]
10. Atici, F.M.; Eloe, P.W. Initial value problems in discrete fractional calculus. *Proc. Am. Math. Soc.* **2009**, *137*, 981–989. [[CrossRef](#)]
11. Abu-Saris, R.; Al-Mdallal, Q. On the asymptotic stability of linear system of fractional-order difference equations. *Fract. Calc. Appl. Anal.* **2013**, *16*, 613–629. [[CrossRef](#)]
12. Mohan, J.J.; Deekshitulu, G.V.S.R. Fractional order difference equations. *Int. J. Differ. Equ.* **2012**, *2012*, 780619. [[CrossRef](#)]
13. Wyrwas, M.; Mozyrska, D.; Girejko, E. Stability of discrete fractional-order nonlinear systems with the nabla caputo difference. *IFAC Proc.* **2013**, *46*, 167–171. [[CrossRef](#)]
14. Edelman, M. Fractional maps and fractional attractors part I: α -families of maps. *Discontin. Nonlinearity Complex.* **2013**, *1*, 305–324. [[CrossRef](#)]
15. Edelman, M. Fractional maps and fractional attractors part II: Fractional difference α -families of maps. *Discont. Nonlinearity Complex.* **2015**, *4*, 391–402. [[CrossRef](#)]
16. Wu, G.C.; Baleanu, D. Discrete fractional logistic map and its chaos. *Nonlinear Dyn.* **2014**, *75*, 283–287. [[CrossRef](#)]
17. Wu, G.C.; Baleanu, D. Discrete chaos in fractional delayed logistic maps. *Nonlinear Dyn.* **2015**, *80*, 1697–1703. [[CrossRef](#)]
18. Wu, G.C.; Baleanu, D. Jacobian matrix algorithm for Lyapunov exponents of the discrete fractional maps. *Commun. Nonlinear Sci. Numer. Simulat.* **2015**, *22*, 95–100. [[CrossRef](#)]
19. Zhang, Y.Q.; Hao, J.L.; Wang, X.Y. An efficient image encryption scheme based on S-boxes and fractional-order differential logistic map. *IEEE Access* **2020**, *8*, 54175–54188. [[CrossRef](#)]
20. Ouannas, A.; Khennaoui, A.; Wang, X.; Pham, V.T.; Boulaaras, S.; Momani, S. Bifurcation and chaos in the fractional form of Hénon-Lozi type map. *Eur. Phys. J. Spec. Top.* **2020**, *229*, 2261–2273. [[CrossRef](#)]
21. Liu, Z.Y.; Xia, T.; Wang, Y.P. Image encryption technique based on new two-dimensional fractional-order discrete chaotic map and Menezes-Vanstone elliptic curve cryptosystem. *Chin. Phys. B* **2018**, *27*, 030502. [[CrossRef](#)]
22. Wang, L.; Sun, K.; Peng, Y.; He, S. Chaos and complexity in a fractional-order higher-dimensional multicavity chaotic map. *Chaos Soliton. Fract.* **2019**, *131*, 109488. [[CrossRef](#)]
23. Jafari, S.; Pham, V.T.; Golpayegani, S.M.R.H.; Moghtadaei, M.; Kingni, S.T. The relationship between chaotic maps and some chaotic systems with hidden attractors. *Int. J. Bifurcat. Chaos* **2016**, *26*, 1650211. [[CrossRef](#)]
24. Cui, L.; Luo, W.H.; Ou, Q.L. Analysis and implementation of new fractional-order multi-scroll hidden attractors. *Chin. Phys. B* **2021**, *30*, 020501. [[CrossRef](#)]
25. Chowdhury, S.N.; Ghosh, D. Hidden attractors: A new chaotic system without equilibria. *Eur. Phys. J. Spec. Top.* **2020**, *229*, 1299–1308. [[CrossRef](#)]
26. Jafari, S.; Sprott, J.C.; Nazarimehr, F. Recent new examples of hidden attractors. *Eur. Phys. J. Spec. Top.* **2015**, *224*, 1469–1475. [[CrossRef](#)]
27. Leonov, G.A.; Kuznetsov, N.V. Hidden attractors in dynamical systems: From hidden oscillation in Hilbert-Kolmogorov, Aizerman and Kalman problems to hidden chaotic attractor in Chua circuits. *Int. J. Bifurcat. Chaos* **2013**, *23*, 1330002. [[CrossRef](#)]
28. Leonov, G.A.; Kuznetsov, N.V.; Vagitsev, V.I. Hidden attractor in smooth Chua systems. *Phys. D* **2012**, *241*, 1482–1486. [[CrossRef](#)]
29. Leonov, G.A.; Kuznetsov, N.V.; Vagitsev, V.I. Localization of hidden Chua's attractors. *Phys. Lett. A* **2011**, *375*, 2230–2233. [[CrossRef](#)]
30. Abdeljawad, T. On Riemann and Caputo fractional differences. *Comput. Math. Appl.* **2011**, *62*, 1602–1611. [[CrossRef](#)]
31. Chen, F.; Luo, X.; Zhou, Y. Existence results for nonlinear fractional difference equation. *Adv. Differ. Equ.* **2011**, *2011*, 713201. [[CrossRef](#)]
32. Ouannas, A.; Khennaoui, A.A.; Momani, S.; Pham, V.T.; El-Khazali, R. Hidden attractors in a new fractional-order discrete system: Chaos, complexity, entropy, and control. *Chin. Phys. B* **2020**, *29*, 050504. [[CrossRef](#)]
33. Khennaoui, A.A.; Ouannas, A.; Boulaaras, S.; Pham, V.T.; Azar, A.T. A fractional map with hidden attractors: Chaos and control. *Eur. Phys. J. Spec. Top.* **2020**, *229*, 1083–1093. [[CrossRef](#)]
34. Sun, K.H.; Liu, X.; Zhu, C.X. The 0-1 test algorithm for chaos and its applications. *Chin. Phys. B* **2010**, *19*, 110510. [[CrossRef](#)]

35. Staniczenko, P.P.A.; Lee, C.F.; Jones, N.S. Rapidly detecting disorder in rhythmic biological signals: A spectral entropy measure to identify cardiac arrhythmias. *Phys. Rev. E* **2009**, *79*, 011915. [[CrossRef](#)]
36. Pincus, S.M. Approximate entropy as a measure of system complexity. *Proc. Natl. Acad. Sci. USA* **1991**, *88*, 2297–2301. [[CrossRef](#)] [[PubMed](#)]
37. Li, X.; Chu, Y.; Liu, X.; Zhang, J. Control discrete (hyper-)chaotic system using improved wavelet functions. *J. Huazhong Univ. Sci. Tech.* **2009**, *37*, 72–74.

Disclaimer/Publisher’s Note: The statements, opinions and data contained in all publications are solely those of the individual author(s) and contributor(s) and not of MDPI and/or the editor(s). MDPI and/or the editor(s) disclaim responsibility for any injury to people or property resulting from any ideas, methods, instructions or products referred to in the content.